ACS Catalysis

Research Article

pubs.acs.org/acscatalysis

Investigating the Electrocatalytic Oxidation of Dihydronicotinamide Adenine Dinucleotide at Nitrogen-Doped Carbon Nanotube Electrodes: Implications to Electrochemically Measuring Dehydrogenase Enzyme Kinetics

Jacob M. Goran, Carlos A. Favela, and Keith J. Stevenson*

Department of Chemistry, Center for Nano- and Molecular Science and Technology, The University of Texas at Austin, 105 East 24th Street, Stop A5300, Austin, Texas 78712-1224, United States

Supporting Information

ABSTRACT: Nitrogen-doped carbon nanotubes (N-CNTs) have been shown to be electrocatalytic toward the oxidation of dihydronicotinamide adenine dinucleotide (NADH), the reduced form of the coenzyme necessary for enzymatic turnover in NAD^+-dependent dehydrogenases. The observed oxidation potential of the electrocatalyst, however, still shows a significant overpotential, suggesting that even for effective electrocatalysts, electrooxidation may be kinetically controlled. We demonstrate using the Koutecky–Levich rotating disk electrode technique that the observed electron transfer rate constant (k_{obs}) is a function of potential over a wide potential window; however, k_{obs} could only be accurately measured for a portion of that window for the electrocatalytic N-CNTs. More importantly, electrochemically measured enzyme kinetics, acquired after adsorption of glucose dehydrogenase onto the N-CNTs, are never independent of potential, even when the electron transfer rate constant is too fast to measure by the rotating disk technique. Thus, electrochemically obtained kinetics (e.g., K_M^{app} and V_{max}) are actually measuring the electrochemical kinetics of NADH oxidation at the electrode surface, rather than the spontaneous and potential-independent enzymatic turnover.

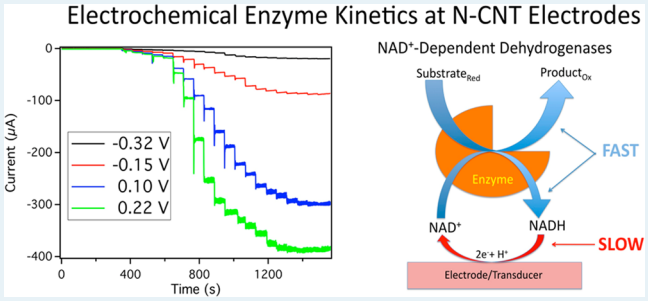

KEYWORDS: *dihydronicotinamide adenine dinucleotide, NADH, enzyme kinetics, dehydrogenases, nitrogen-doped carbon nanotubes, carbon nanotubes, Michaelis–Menten kinetics*

INTRODUCTION

Carbon nanomaterials such as carbon nanotubes (CNTs) and graphene are increasingly being coupled with enzymes to create bioelectrodes[1] for biosensing[2−5] and biofuel cell[6−8] applications. Enzymes incorporated into an electrode impart a biorecognition element that is selective to a specific substrate or fuel in the case of biofuel cell electrodes. NAD^+-dependent dehydrogenase enzymes are one of the more commonly applied enzymes, requiring the cofactor nicotinamide adenine dinucleotide (NAD^+) in conjunction with an appropriate substrate to cause enzymatic turnover. The general enzymatic reaction for a NAD^+-dependent dehydrogenase is shown below:

$$\text{substrate} + NAD^+ \rightarrow \text{product} + NADH \text{ (in the presence of enzyme)} \quad (1)$$

The reduced cofactor, dihydronicotinamide adenine dinucleotide (NADH), can be reoxidized at an electrode surface via a 2-electron one-proton oxidation shown below:

$$NADH \rightarrow NAD^+ + 2e^- + H^+ \quad (2)$$

The formal potential of the NADH/NAD^+ couple is low, at −0.96 V vs Hg/Hg_2SO_4 (−0.52 vs Ag/AgCl; −0.56 vs SCE; −0.32 vs NHE)[9] and requires a large overpotential in order to be observed at conventional electrodes such as Pt or carbon. In order to lower the overpotential, mediators or catalysts are employed.[10,11] CNTs have been shown to be electrocatalytic toward NADH oxidation by substantially lowering the overpotential compared to conventional glassy carbon.[12−19] Often, CNTs are coupled with mediators to further lower the oxidation overpotential.[20−24] Mediators are polymerized on the CNT surface, or dispersed within a polymer, biopolymer, or hydrogel matrix to effectively couple the individual components and create a biocompatible environment for enzyme immobilization.[25−37] Heteroatom-doped CNTs, both B-CNTs[38] and N-CNTs,[39] have been shown to further decrease the oxidation overpotential compared to nondoped CNTs, without additional mediation. Although many reports have touted the benefits of CNTs for NADH oxidation, or demonstrated their use with dehydrogenases, the electron transfer kinetics of the electrochemical reaction are often neglected. This aspect is increasingly important since many reports are evaluating the enzymatic behavior of the bioelectrode by electrochemically

Received: March 15, 2014
Published: July 24, 2014

   dx.doi.org/10.1021/cs5006794 | ACS Catal. 2014, 4, 2969−2976

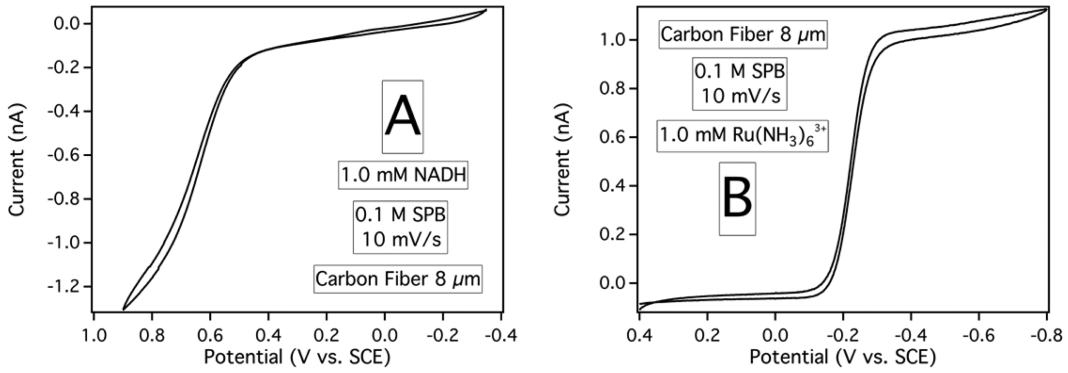

Figure 1. Oxidation of 1.0 mM NADH (A) or the reduction of 1.0 mM $Ru(NH_3)^{3+}$ (B) at an 8 μm carbon fiber UME (0.1 M SPB, pH 7.0, scan rate 10 mV/s).

measuring the enzyme kinetics.[40−50] Thus, it is imperative to ensure that the electron transfer kinetics at the electrode surface are not a limiting factor in the kinetic analysis of the enzyme. The physical distance of the catalytic redox site embedded in most enzymes prevents the direct electron transfer between the redox site and the electrode.[6,51,52] The electric field emanating from the electrode surface, then, should have a negligible influence on the enzymatic reaction, which is mainly dependent on the substrate concentration. The vast majority of electrochemically determined enzyme kinetics (e.g., K_M^{app} and V_{max}) are performed at a single potential, neglecting to demonstrate potential-independence of the enzymatic reaction, or attempting to identify the influence of potential on the electrochemical reaction. Herein, we report a kinetic evaluation of NADH oxidation at electrocatalytic N-CNT electrodes. Additionally, we allow glucose dehydrogenase (GDH) to spontaneously adsorb onto the N-CNT surface and evaluate the enzyme kinetics via NADH oxidation. This study is beneficial to understanding the fundamental reactivity of N-CNTs since dispersing agents, binders, redox mediators, oxidizing acids, and immobilizing matrices (polymer, biopolymer, or hydrogel matrix) are not used. We identify a potential region where the electron transfer rate constant is too rapid to accurately measure by the rotating disk electrode technique, and should supply accurate enzyme kinetics, but find that the obtained measurements are still under the kinetic control of the electrochemical reaction. Beyond this potential region, application of the enzyme by spontaneous adsorption is limited due to the oxidation of the N-CNT electrode surface, which causes the adsorbed enzyme to detach from the electrode surface.

EXPERIMENTAL SECTION

Enzyme and Chemicals. Glucose Dehydrogenase (from *Pseudomonas* sp., E.C. 1.1.1.47, lyophilized powder ≥200 U/mg), β-nicotinamide adenine dinucleotide dipotassium salt, α-D-glucose, and *m*-xylene (anhydrous) were obtained from Sigma-Aldrich. Sodium phosphate monobasic (NaH_2PO_4, monohydrate), sodium phosphate dibasic (Na_2HPO_4, anhydrous), pyridine, pH calibration buffers (4.00, 7.00, 10.00), and sodium hydroxide were purchased from Fisher. Bis(cyclopentadienyl)iron (ferrocene) was obtained from Alfa Aesar. Hexaammineruthenium(III) chloride (99%) was purchased from Strem Chemicals.

N-CNT Synthesis. N-CNTs were synthesized by injecting a 20 mg mL^{-1} solution of ferrocene dissolved in pyridine at 0.1 mL min^{-1} via a glass syringe (Hamilton 81320) and an automated syringe pump (New Era Pump Systems NE-1000) into a quartz tube laid lengthwise across two identical tube furnaces (Carbolite model HST 12/35/200/2416CG). The first furnace, where the solution entered the tube, was set at 130 °C to ensure the catalyst solution entered the vapor phase. The second furnace was set at 800 °C to cause the vapor to deposit multiwalled N-CNTs on the inside lining of the quartz tube via a floating catalyst chemical vapor deposition (CVD) process. Argon was used as a carrier gas (532 sccm) to direct the flow of the catalyst solution from the first tube furnace to the second, with the coinjection of ammonia (43 sccm), controlled by two gas mass flow controllers (MKS type 1179A) for a total gas flow of 575 sccm. N-CNTs made by this process contain 7.4 atom % N.

Electrochemistry, Electrode Preparation, and Spectrophotometry. Electrochemical information is presented with a positive cathodic current and a negative anodic current. Ultramicroelectrode (UME) cyclic voltammograms were obtained with a CH Instruments 700A potentiostat in conjunction with a SCE reference electrode, and a platinum wire counter electrode, all inside a CH Instruments Faraday cage. All other electrochemical measurements were performed with an Autolab PGSTAT30 potentiostat (GPES software version 4.9) in coordination with a five-neck glass cell (125 mL), a Hg/Hg_2SO_4 reference electrode (CH Instruments, +0.64 V vs SHE; +0.44 V vs Ag/AgCl; +0.40 V vs SCE), and a coiled Au counter electrode. Potentials are reported vs Hg/Hg_2SO_4 unless noted otherwise (such as in the UME section). Rotating disk electrode (RDE) experiments were performed on a Pine Instruments AFMSRX rotator. N-CNT electrodes were prepared by drop casting a 12 μL aliquot of a 2 mg mL^{-1} solution of N-CNTs in absolute ethanol (sonicated for 2 h) onto a 0.5 cm diameter glassy carbon RDE (Pine Instruments AFE2M050GC). GC electrodes which were polished with a 0.05 μm alumina slurry on microcloth (Buehler) and briefly sonicated in 18 MΩ cm water to remove adsorbed alumina prior to use or N-CNT application. N-CNT electrodes were "wet" in a mixture of ethanol and 0.1 M sodium phosphate buffer (SPB) to ensure complete surface contact with the electrolyte solution. N-CNT electrodes were also cycled between 0 and −1.2 V to passivate electroactive iron remaining from the CVD synthesis.[53] NADH concentrations for electrochemical experiments were calculated on the basis of mass, which may underestimate the actual concentration. Spectrophotometric analysis was performed on an Agilent 8453 UV−visible (UV−vis) spectrophotometer (photodiode array) using quartz cuvettes (path length of 1 cm). Glucose dehydrogenase

dx.doi.org/10.1021/cs5006794 | ACS Catal. 2014, 4, 2969−2976

and NAD^+ were added to the cuvette prior to the introduction of glucose for all UV−vis measurements. NADH concentrations via UV−vis absorbance at 340 nm were calculated with a molar extinction coefficient of 6200 M^{-1} cm^{-1}, a value similar to that in other reports.[45,54] Spontaneous adsorption of GDH onto N-CNTs was done at room temperature. When not in use, GDH solutions were stored at 4 °C. Nonlinear Michaelis−Menten enzyme kinetics and Koutecky−Levich rotating disk electrode data were fit using IGOR pro (v. 6.12).

RESULTS AND DISCUSSION

Oxidation of NADH at Carbon Fiber Ultramicroelectrodes: A Qualitative Study. Ultramicroelectrodes (UMEs) are a useful tool for evaluating the electron transfer kinetics of redox molecules due to their increased mass transport via radial diffusion. Figure 1 presents a cyclic voltammogram (CV) of a 8 μm carbon fiber electrode in the presence of 1.0 mM NADH or 1.0 mM ruthenium hexamine ($Ru(NH_3)_6^{3+}$) in 0.1 M sodium phosphate buffer (SPB) at a pH of 7.0. The reduction of $Ru(NH_3)_6^{3+}$ displays a typical sigmoidal shape with a mass transfer limited plateau, not seen in the NADH oxidation CV. The missing plateau can be explained if the electron transfer reaction for NADH oxidation is kinetically limited, rather than mass transfer limited like the $Ru(NH_3)_6^{3+}$.

More importantly, the ideal outer sphere redox couple $Ru(NH_3)_6^{3+/2+}$ displays a nearly flat baseline before reduction, $E_{1/2}$ at −0.2 (V vs SCE), with a rapid attainment of a mass transfer controlled plateau. NADH, on the other hand, displays a sloping background before the E_p, close to 0.6 (V vs SCE), and does not attain a limiting current within the measurement. Furthermore, the reduction of $Ru(NH_3)_6^{3+}$ is a one-electron reaction, while the oxidation of NADH is a 2-electron oxidation, even though the current magnitude for both reactions is similar (diffusion will be slightly slower for the larger NADH molecule). Qualitatively, the data suggest that NADH oxidation is kinetically limited rather than mass transport limited.

The Potential Dependent Observed Electron Transfer Rate Constant (k_{obs}). Our prior report identified the E_p for the oxidation of NADH at N-CNTs (7.4 atom % N) and GC at −0.32 and 0.22 (V vs Hg/Hg_2SO_4), respectively, in 0.1 M SPB (pH 7.0) at a scan rate of 10 mV/s in the presence of 2.0 mM NADH.[39] In order to further quantify the electron transfer kinetics of the NADH reaction, five potentials were chosen to perform Koutecky−Levich rotating disk electrode (RDE) analysis, which is capable of differentiating a kinetically limited process from a mass transport limited process. The mass transfer limiting current at a RDE is defined by the Levich equation, shown below:[55]

$$i_{mt} = 0.62nFAD^{2/3}\omega^{1/2}\nu^{-1/6}C \quad (3)$$

where i_{mt} is the mass transfer limiting current, n is the number of electrons transferred ($n = 2$), F is Faraday's constant (96,485 C/mol), A is the electrode area, ω is the angular velocity ($\omega = 2\pi f$; f is frequency), ν is the kinematic viscosity of the solvent (water in this case, 0.01 cm^2/s), C is the concentration of NADH, and D is the diffusion coefficient. The diffusion coefficient was selected as 3.0×10^{-6} cm^2/s based on literature references.[19,34,56−58] The measured current (i) may not align with i_{mt} if the reaction is limited by the electron transfer kinetics rather than mass transport. In this case, a plot of i vs $\omega^{1/2}$ should yield an asymptote approaching the kinetically limiting current i_K. The kinetically limiting current is also a function of potential (E), shown below:[55]

$$i_K = nFAk_{obs}(E)C \quad (4)$$

where i_K is the kinetically limited current, k_{obs} is the observed electron transfer rate constant (a function of E) and F, A, n, and C are the same as mentioned above. A plot of $1/i$ vs $1/\omega^{1/2}$ allows one to determine the asymptote i_K, which will be the y-intercept (a mass transport limited plot will theoretically intercept the y-axis at 0). The measured current (i) can be expressed from the Koutecky−Levich equation shown below:

$$1/i = 1/i_K + 1/i_{mt} \quad (5)$$

where the measured current (i) is a function of both the mass transport limited current (i_{mt}) and the kinetically limited current (i_K). Likewise, one can use nonlinear fitting to approximate the asymptote directly from the plot of i vs $\omega^{1/2}$. The nonlinear method will avoid errors introduced from linearization, which will be discussed later. Practically, one must be able to rotate at high rates in order to observe the asymptotic behavior for relatively fast k_{obs}, setting an upper limit on our measuring capabilities. Nonetheless, we used RDE amperometry to ascertain the k_{obs} as a function of potential and concentration at a conventional GC electrode, or an electrocatalytic material, N-CNTs. Figure 2A presents CVs of a GC and a N-CNT electrode in the presence of 2.0 mM NADH, and includes the potentials chosen to perform RDE analysis. Parts C and B of Figure 2 present representative chronoamperograms of the RDE analysis for a series of N-CNT electrodes at 1.0 mM NADH (Figure 2B) and a series of GC electrodes at 0.5 mM NADH (Figure 2C).

According to the CVs in Figure 2A, the rate constant for N-CNTs should be relatively fast, since they are all at or past the observed E_p. At GC, the selected potentials span the entire range. The negative potentials are before the reaction begins, 0.10 V is near the onset of E_p, and the most positive two potentials are at and beyond the E_p. Since the overpotential for NADH oxidation is much lower on N-CNTs than on GC, we expect the rate constant to be faster at all potentials for the N-CNTs. The initial spike at 300 s in Figure 2B and 2C is where the NADH was introduced into solution at the lowest rotation rate of 250 rpm. Subsequent current steps are due to an increase in the rotation rate. The NADH spike at 300 s, rather than having NADH in solution during the entire experiment, was used to minimize NADH contact prior to obtaining a measurement, since NADH is known to foul the electrode surface.[9−11] In order to determine if the concentration of NADH influences the accuracy of the obtained rate constant (k_{obs}) due to electrode fouling, RDE analysis was performed at three different NADH concentrations (0.1, 0.5, and 1.0 mM). Table 1 and Table 2 present the calculated k_{obs} values as a function of potential and concentration for both GC and N-CNT electrodes, respectively, using nonlinear fitting to determine i_K (and hence, k_{obs}) and the associated error from the nonlinear fit. Table T1 and T2 in the Supporting Information (SI) present the k_{obs} values determined from the traditional Koutecky−Levich linear analysis. It is clear from the CVs in Figure 2 and the k_{obs} values in Table 1 and Table 2 that N-CNTs catalyze the oxidation of NADH at much lower potentials than GC. The oxidation reaction is not observed at GC below 0.10 V, while above 0.10 V the reaction at N-CNTs is too fast to measure using the RDE technique (highest rotation rate of 5000 rpm), since an asymptote is not observed.

dx.doi.org/10.1021/cs5006794 | ACS Catal. 2014, 4, 2969−2976

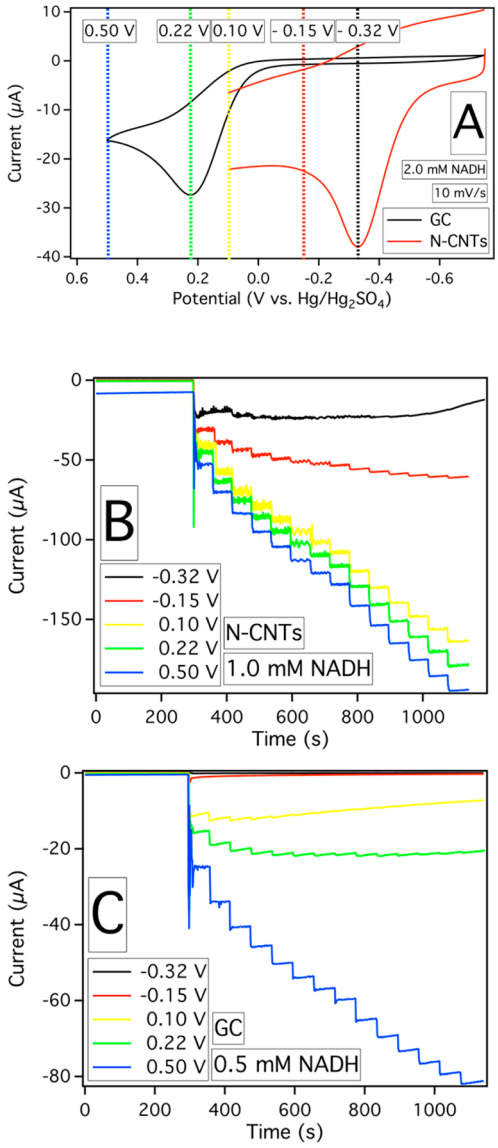

Figure 2. (A) CVs of a GC or a N-CNT electrode in the presence of 2.0 mM NADH in 0.1 M SPB (colored dashed lines mark the selected potentials for RDE measurements). Chronoamperograms for a series of N-CNT electrodes in the presence of (B) 1.0 mM NADH or a series of GC electrodes in the presence of (C) 0.5 mM NADH as the rotation rate is increased (from 250 to 5000 rpm).

The SI Figure S1 displays RDE data for N-CNTs at 0.5 mM NADH for −0.32, −0.15, and 0.10 V, along with their respective nonlinear fits. At more positive potentials, there is less data to fit to an asymptote, so the extrapolated limiting current (and associated k_{obs} value) has greater uncertainty even though the error in the fit may be reasonable. We have shown the values of k_{obs} for 0.10 V at N-CNTs in Table 2 to verify that any apparent trends continue but admit that these values are fairly uncertain.

Table 2. k_{obs} (1×10^{-3} cm/s) Values As a Function of Potential and Concentration at N-CNTs

	potential (V vs Hg/Hg_2SO_4)				
	−0.32	−0.15	0.10	0.22	0.50
0.1 mM NADH	2.8 ± 0.1	8.9 ± 0.1	90 ± 20[a]	NM[b]	NM[b]
0.5 mM NADH	1.29 ± 0.01	4.09 ± 0.03	38 ± 1[a]	NM[b]	NM[b]
1.0 mM NADH	0.91 ± 0.01	2.67 ± 0.02	31 ± 3[a]	NM[b]	NM[b]

[a]These values are presented to verify apparent trends, but are extrapolated from a nearly linear fit. [b]NM = Not Measured. This indicates that for the rotation rates used here, an asymptote was not observed, and the reaction is apparently mass transfer limited.

The k_{obs} values show a concurrent increase with potential at any given concentration, but a decreasing k_{obs} with increasing NADH concentration at the same potential. The inverse relationship of the rate constant to NADH concentration at a constant potential has also been observed at MWCNT electrodes modified with 2,3,5,6-tetrachloro-1,4-benzoquinone,[23] polyxanthurenic acid,[34] and 3,5-dinitrobenzoic acid,[59] or SWCNT electrodes modified with Nile Blue[60] or poly(phenosafranin).[61] The aforementioned electrodes all used mediators, often called chemically modified or mediator-modified electrodes. The inverse relationship of the rate constant to the NADH concentration at these mediator-modified electrodes has been characterized by Gorton, who identifies the rate -limiting step as a charge transfer complex between NADH and the surface bound mediator.[10,11] The complex essentially mimics the Michaelis−Menten kinetics of an enzyme, where the substrate-bound enzyme limits the enzymatic turnover. Although there is not an observable surface wave indicating an electroactive mediator at our N-CNTs, they still may include a mediating surface site, since nitrogen incorporated into an all-carbon lattice significantly influences the electron distribution and can also introduce nitrogen functional groups.[62−65] The data presented here preclude an accurate analysis of the type characterized by Gorton, but it should be further investigated, taking note that unmodified GC also displays a similar effect.

Response currents from the introduction of NADH at a constant rotation rate can also be used to show the potential dependence of the NADH oxidation current. Figure 3 presents a series of RDE chronoamperograms for N-CNT electrodes obtained at the five selected potentials as 0.5 mM NADH was introduced into solution. Tables 3 and 4 present the current as a percent of the theoretical current, calculated from eq 3, using the geometric area of the GC electrode for both the GC and N-CNT electrodes (0.196 cm^2), since solution-based electroactive species interact with the same effective area on both electrodes.[66]

Table 1. k_{obs} (1×10^{-3} cm/s) Values As a Function of Potential and Concentration at GC

	potential (V vs Hg/Hg_2SO_4)				
	−0.32	−0.15	0.10	0.22	0.50
0.1 mM NADH	no reaction	no reaction	4.789 ± 0.002	5.063 ± 0.004	38 ± 1
0.5 mM NADH	no reaction	no reaction	0.98 ± 0.02	1.88 ± 0.03	15.8 ± 0.2
1.0 mM NADH	no reaction	no reaction	0.297 ± 0.003	1.82 ± 0.02	5.89 ± 0.03

dx.doi.org/10.1021/cs5006794 | ACS Catal. 2014, 4, 2969−2976

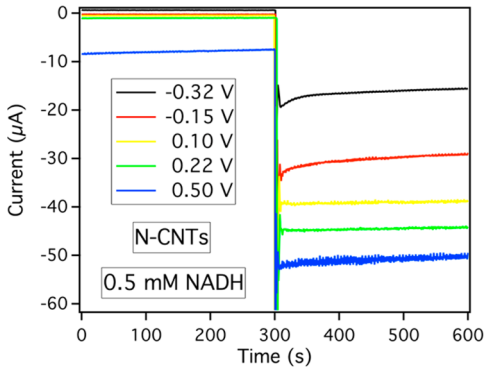

Figure 3. Chronoamperograms of the oxidation of 0.5 mM NADH at N-CNT electrodes as they are rotated at 1000 rpm (0.1 M SPB, pH 7.0).

Table 3. Percent of Theoretical Current As a Function of Potential and Concentration at GC

	potential (V vs Hg/Hg_2SO_4)				
	−0.32	−0.15	0.10	0.22	0.50
0.1 mM NADH	0.23%	1.7%	37%	78%	86%
0.5 mM NADH	0.05%	0.43%	24%	63%	86%
1.0 mM NADH	0.05%	0.06%	44%	75%	84%

Table 4. Percent of Theoretical Current As a Function of Potential and Concentration at N-CNTs

	potential (V vs Hg/Hg_2SO_4)				
	−0.32	−0.15	0.10	0.22	0.50
0.1 mM NADH	61%	65%	75%	83%	84%
0.5 mM NADH	35%	60%	73%	81%	83%
1.0 mM NADH	31%	49%	69%	75%	79%

The current response for GC is not as monotonic as the N-CNTs, which display an increase in the current response concurrent with potential and inversely related to NADH concentration. For GC, there is almost no current response before 0.10 V, expected since it is before the onset of NADH oxidation at GC. Both GC and N-CNTs tend toward a limit of about 85% of the theoretical current at high potentials, verifying that the same effective surface area is utilized by NADH at both electrodes. The identical upper limit also suggests that either the initial surface fouling at higher potentials is similar, and/or the diffusion coefficient is underestimated. It should be noted that the anodic background current at 0.50 V on N-CNTs is significantly higher than the other potentials, or the GC electrode. The background current at both GC and N-CNT electrodes increases slightly (more anodic) concomitant with potential, shown in the SI in Figure S2(A−D) for the smaller 0.1 mM NADH current responses. The higher current at 0.50 V and subsequent decay before NADH is introduced suggests that at this potential (and beyond) the carbon is being oxidized. This phenomenon will have a significant impact when enzymes are adsorbed on the N-CNT surface, where the oxidizing carbon will cause the adsorbed enzyme to disengage from the electrode surface.

Spectrophotometric Enzyme Kinetics. The standard method to measure the activity of glucose dehydrogenase, and many other NAD^+-dependent dehydrogenase enzymes, is to monitor the appearance of NADH from the enzymatic turnover of NAD^+ and glucose (or an appropriate substrate for other NAD^+-dependent dehydrogenase enzymes). NADH absorbs at 340 nm, due to the pyridinic ring in nicotinamide, with an molar extinction coefficient of about 6200 M^{-1} cm^{-1}.[54] For enzymes purchased from a reputable company, and usually for the sake of time, only one very high substrate concentration is performed at a high temperature (37 °C) and optimal pH, buffer, and buffer ionic strength to obtain the specific activity which is defined by the company. In order to obtain a more comprehensive kinetic analysis, a series of concentrations must be characterized, where the initial enzyme activity increases with the concentration of substrate until it reaches an asymptote, where the rate is nearly independent of concentration. Figure 4(A−D) presents the series of spectrophotometric analyses for GDH in 0.1 M SPB with 2.0 mM NAD^+.

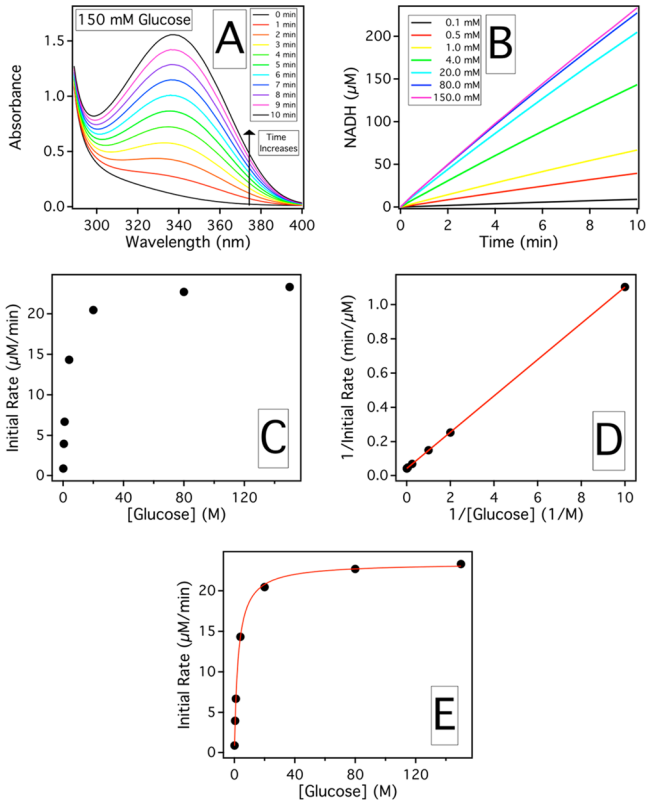

Figure 4. (A) UV−vis spectra displaying the increase in absorbance as a function of time and concentration of glucose. (B) Increase in NADH concentration as a function of glucose concentration displaying linearity in the 10 min time frame. (C) Plot of glucose concentration versus initial rate (first 10 min). (D) Lineweaver−Burk plot of the inverse glucose concentration versus the inverse initial rate. (E) Nonlinear fitting of the substrate saturation curve. (GDH 8 nM, 0.1 M SPB, pH 7.0, 2.0 mM NAD^+).

The kinetic parameters K_M and V_{max} can be calculated from the *y*-intercept and the slope of the Lineweaver−Burk plot (shown in Figure 4D) or by nonlinear fitting (shown in Figure 4E). Due to linearization errors from the double reciprocal plot, where the low concentration rates in the bottom left corner of Figure 4C become the most influential points in the top right corner of Figure 4D, we chose to present the data from the nonlinear analysis shown in Figure 4E. Figure S3 in the SI presents the UV−visible spectra of the increasing peak at 340 nm as a function of glucose concentration. Table T3 in the SI presents the Lineweaver−Burk linear analysis of K_M and V_{max}

dx.doi.org/10.1021/cs5006794 | *ACS Catal.* 2014, 4, 2969−2976

along with a modified data set to minimize errors from linearization. Note that, even after the data was modified to eliminate linearization errors, the standard deviation for both K_M and V_{max} are smaller for the nonlinear analysis, compared to the linear analysis. The nonlinear values were determined to be 2.9 ± 0.3 mM for K_M and 4.4 ± 0.8 × 10^{-7} M/s for V_{max}. To ensure that the 2.0 mM NAD^+ concentration did not limit the enzymatic reaction, analysis was also performed in 10.0 mM NAD^+. The kinetic parameters were not statistically differentiable and actually displayed a slightly smaller K_M and V_{max}. Given that 8 nM of GDH was present in solution (based on mass) the k_{cat} can be calculated ($k_{cat} = V_{max}/[GDH]$) at 55 s^{-1}. Over a 74 day period, K_M and V_{max} were not seen to appreciably change, indicating that the enzyme was quite stable in solution. When not in use, the GDH solution was stored in the refrigerator (4 °C). Table T4 in the Supporting Information presents a chart of K_M and V_{max} over the 74 day period.

Electrochemical Enzyme Kinetics. Electrochemically measured enzyme kinetics are actually quite a bit easier to obtain than the standard spectrophotometric analysis. The enzymatic rate for each glucose concentration is simply the steady-state current of the bioelectrode at each glucose concentration. The entire saturation curve can be obtained in a single experiment, rather than multiple experiments at different substrate concentrations. The measured signal, however, is now created from the electrochemical oxidation of the enzymatically generated NADH at the N-CNT surface. This is a current density (A/cm^2), rather than a concentration measurement (M), since the measured current is coming from an area, not a volume. Herein lies the fundamental problem of matching up enzyme kinetics obtained electrochemically with those obtained spectrophotometrically, V_{max} will be in different units. The K_M values can be compared directly, since they are both in identical units (M).[67] The k_{cat} can be calculated if the concentration of enzyme is known or the surface coverage of the enzyme on the electrode is known. If adsorbed GDH and free GDH behave identically (have the same k_{cat}) then k_{cat} determined spectrophotometrically can be used to determine the amount of enzyme on the electrode surface.

Enzyme kinetics were measured electrochemically by allowing GDH to adsorb onto the surface of N-CNTs, and subsequently performing substrate saturation curves by amperometric detection. A prior report showed that allowing GDH to adsorb onto the N-CNT surface for 20 min in a 20 μM GDH solution (0.1 M SPB, pH 7.0) gave the bioelectrode the highest current sensitivity (A M^{-1} cm^{-2}) to glucose.[39] Thus, N-CNT electrodes were allowed to adsorb GDH from a 20 μM solution for 20 min. Figure 5 presents chronoamperograms of the electrochemically measured enzyme substrate saturation curves at the five selected potentials for the GDH loaded N-CNT electrodes. Table 5 presents the electrochemically determined K_M^{app} and V_{max} (by nonlinear analysis using the Michaelis–Menten kinetic model) as well as the bioelectrode's sensitivity to glucose at each poised potential. Figure S4 in the SI displays representative plots of the Lineaweaver-Burk linear fitting versus the nonlinear fitting for each of the selected potentials. The residuals of each fit, included in Figure S4 in the SI, show that the majority of the error in the linear fit comes from the initial points of the original (nonlinearized) data, whereas the error in the nonlinear fit are more evenly distributed. Table T5 in the SI presents K_M^{app} and V_{max} determined from the Lineweaver–Burk linear analysis from the full data set, or a modified data set in order to minimize linearization errors.

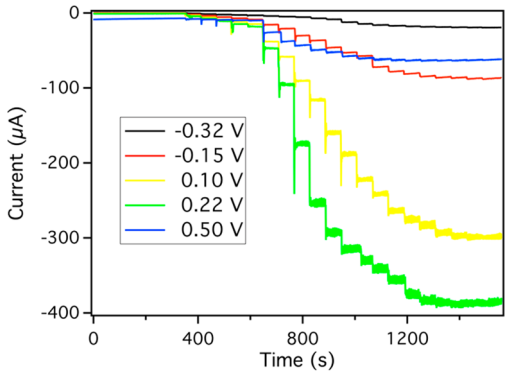

Figure 5. Chronoamperograms of the GDH-loaded N-CNT electrodes at increasing potentials as glucose is introduced into solution (0.1 M SPB, pH 7.0, 1000 rpm).

Table 5. K_M^{app} and V_{max} and the Sensitivity of the GDH Electrode to Glucose

potential (V vs Hg/Hg_2SO_4)	sensitivity (A M^{-1} cm^{-2})	K_M^{app} (mM)	V_{max} (1×10^{-10} mol/s)
−0.32	0.029 ± 0.005	3.0 ± 0.2	1.0 ± 0.2
−0.15	0.074 ± 0.007	5.1 ± 0.7	4 ± 2
0.10	0.13 ± 0.01	12.6 ± 0.7	18 ± 1
0.22	0.14 ± 0.02	15.0 ± 0.9	22 ± 2
0.50	0.018 ± 0.009	20 ± 6	3 ± 1

As mentioned before, the enzyme should be unaffected by the electrode potential, and thus, only controlled by the concentration of substrate in solution. Figure 5 and Table 5 clearly show an increase in both K_M^{app} and V_{max} concurrent with increasing potential until 0.50 V, which breaks from the increasing trend. Since the amount of enzyme on every electrode is similar, and the enzyme should not be influenced by the potential, the increasing kinetic parameters indicate that the electrochemical reaction of NADH, even at an electrocatalyst like N-CNTs, is the rate-limiting reaction. Thus, electrochemically measured enzyme kinetics obtained from the oxidation of NADH created from the enzymatic turnover of NAD^+-dependent dehydrogenases are not independent of potential. It is simply circumstance that the K_M obtained spectrophotometrically and the electrochemical K_M^{app} at −0.32 V are nearly identical.

In order to determine the root cause of the discrepancy at 0.50 V, which was not observed to break trend during the RDE analysis, electrochemical enzyme substrate saturation curves were performed at 0.22 V, but after the normal 20 min of GDH adsorption, the electrodes were then pretreated at 0.22 or 0.50 for 30 min (electrodes are under potential for 26 min during a normal electrochemical measurement). Additionally, GDH was only allowed to adsorb for 3 min or 30 s on two other N-CNT electrodes, as a comparison. Figure 6 presents the results of performing the substrate saturation curves on all four electrodes.

The K_M^{app} for the various adsorption times (30 s, 3 min, and 20 min pretreated at 0.22 V) were within the standard deviation of the normal K_M^{app} for 20 min of adsorption and analysis at 0.22 V. These data indicate that at a single potential (0.22 V), the K_M^{app} is independent of the amount of enzyme adsorbed on the surface, expected for a Michaelis–Menten-type behavior.

dx.doi.org/10.1021/cs5006794 | ACS Catal. 2014, 4, 2969–2976

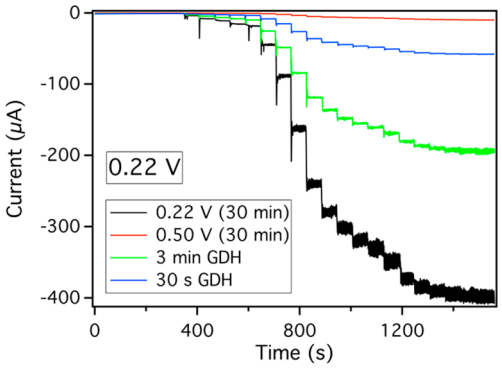

Figure 6. Chronoamperograms of the substrate saturation curves obtained at 0.22 V for the GDH loaded N-CNT electrodes pretreated at 0.50 and 0.22 V, or allowed to adsorb GDH for only 3 min or 30 s (1000 rpm, 0.1 M SPB, pH 7.0).

Figure 6 also shows that the amount of enzyme remaining on the 0.50 V pretreated electrode has significantly decreased, less than the electrode with only 30 s of GDH adsorption. The background anodic signal at 0.50 V (Figure 5) is significantly higher, indicating that something is getting oxidized. Since the high anodic background current is observed without the presence of redox active species (Figure S2C in the SI), the most likely source of the oxidation current is from the N-CNTs. This observation is corroborated by the low V_{max}, suggesting that GDH is disengaging from the surface as the N-CNTs are being oxidized.

CONCLUSION

The spontaneous adsorption of GDH onto the N-CNT surface provides a simple technique to create bioelectrodes without binders, dispersing agents, immobilizing matrices (polymers, biopolymers, hydrogel, etc.), or the inclusion of redox mediators. The elementary bioelectrodes allow for an unambiguous assessment of the intrinsic reactivity and/or limitations of the electrode/biomolecule system. In regards to NAD^+-dependent dehydrogenases, N-CNTs have been shown to be effective electrocatalysts for NADH oxidation, but the observed rate constant is under potential control. Thus, electrochemically measured enzyme kinetics, which obtain their measurement by the oxidation of NADH, are not reliable indicators of the enzymatic behavior. Albeit, at a single potential, the measured enzyme kinetics can be used as a relative indicator, the obtained kinetic parameters are unique to each potential and are not directly comparable to the enzyme free in solution.

ASSOCIATED CONTENT

Supporting Information

Four figures and five tables as noted in the text. This material is available free of charge via the Internet at http://pubs.acs.org.

AUTHOR INFORMATION

Corresponding Author

*E-mail: Stevenson@cm.utexas.edu

Notes

The authors declare no competing financial interest.

ACKNOWLEDGMENTS

Financial support of this work was provided by the R.A. Welch Foundation (grant F-1529). C.A.F. acknowledges support from NSF-REU program (Grant CHE-1003947). We thank Dr. Radhika Dasari for preparing the carbon fiber UME and her assistance with the UME measurements.

REFERENCES

(1) Walcarius, A.; Minteer, S. D.; Wang, J.; Lin, Y.; Merkoçi, A. *J. Mater. Chem. B* **2013**, *1*, 4878−4908.
(2) Yang, W.; Ratinac, K. R.; Ringer, S. P.; Thordarson, P.; Gooding, J. J.; Braet, F. *Angew. Chem., Int. Ed.* **2010**, *49*, 2114−2138.
(3) Jacobs, C. B.; Peairs, M. J.; Venton, B. J. *Anal. Chim. Acta* **2010**, *662*, 105−127.
(4) Zhu, Z.; Garcia-Gancedo, L.; Flewitt, A. J.; Xie, H.; Moussy, F.; Milne, W. I. *Sensors* **2012**, *12*, 5996−6022.
(5) Vashist, S. K.; Zheng, D.; Al-Rubeaan, K. *Biotechnol. Adv.* **2011**, *29*, 169−188.
(6) Willner, I.; Yan, Y.-M.; Willner, B.; Tel-Vered, R. *Fuel Cells (Weinheim, Ger.)* **2009**, *9*, 7−24.
(7) Meredith, M. T.; Minteer, S. D. *Annu. Rev. Anal. Chem.* **2012**, *5*, 157−179.
(8) Holzinger, M.; Le Goff, A.; Cosnier, S. *Electrochim. Acta* **2012**, *82*, 179−190.
(9) Radoi, A.; Compagnone, D. *Bioelectrochemistry* **2009**, *76*, 126−134.
(10) Gorton, L.; Domínguez, E. *Rev. Mol. Biotechnol.* **2002**, *82*, 371−392.
(11) Gorton, L. *J. Chem. Soc., Faraday Trans. 1* **1986**, *82*, 1245−1258.
(12) Musameh, M.; Wang, J.; Merkoci, A.; Lin, Y. *Electrochem. Commun.* **2002**, *4*, 743−746.
(13) Wang, J.; Deo, R. P.; Poulin, P.; Mangey, M. *J. Am. Chem. Soc.* **2003**, *125*, 14706−14707.
(14) Wang, J.; Musameh, M. *Anal. Chem.* **2003**, *75*, 2075−2079.
(15) Chen, J.; Bao, J.; Cai, C.; Lu, T. *Anal. Chim. Acta* **2004**, *516*, 29−34.
(16) Wooten, M.; Gorski, W. *Anal. Chem.* **2010**, *82*, 1299−1304.
(17) Sun, Y.; Ren, Q.; Liu, X.; Zhao, S.; Qin, Y. *Biosens. Bioelectron.* **2013**, *39*, 289−295.
(18) Lawrence, N.; Deo, R.; Wang, J. *Electroanalysis* **2005**, *17*, 65−72.
(19) Banks, C. E.; Compton, R. G. *Analyst* **2005**, *130*, 1232−1239.
(20) Radoi, A.; Compagnone, D.; Valcarcel, M. A.; Placidi, P.; Materazzi, S.; Moscone, D.; Palleschi, G. *Electrochim. Acta* **2008**, *53*, 2161−2169.
(21) Lawrence, N. S.; Wang, J. *Electrochem. Commun.* **2006**, *8*, 71−76.
(22) Zhu, L.; Zhai, J.; Yang, R.; Tian, C.; Guo, L. *Biosens. Bioelectron.* **2007**, *22*, 2768−2773.
(23) De Cássia Silva Luz, R.; Damos, F. S.; Tanaka, A. A.; Kubota, L. T.; Gushikem, Y. *Electrochim. Acta* **2008**, *53*, 4706−4714.
(24) Neto, S. A.; Almeida, T. *Electroanalysis* **2013**, *25*, 2394−2402.
(25) Zhang, M.; Gorski, W. *Anal. Chem.* **2005**, *77*, 3960−3965.
(26) Zeng, J.; Wei, W.; Wu, L.; Liu, X.; Liu, K.; Li, Y. *J. Electroanal. Chem.* **2006**, *595*, 152−160.
(27) Li, H.; Wen, H.; Calabrese Barton, S. *Electroanalysis* **2012**, *24*, 398−406.
(28) Meredith, M. T.; Giroud, F.; Minteer, S. D. *Electrochim. Acta* **2012**, *72*, 207−214.
(29) Karra, S.; Zhang, M.; Gorski, W. *Anal. Chem.* **2012**, *85*, 1208−1214.
(30) Lin, K. C.; Yin, C. Y.; Chen, S. M. *Analyst* **2012**, *137*, 1378−1383.
(31) Zhang, M.; Gorski, W. *J. Am. Chem. Soc.* **2005**, *127*, 2058−2059.
(32) Gasnier, A.; Pedano, M. L.; Gutierrez, F.; Labbé, P.; Rivas, G. A.; Rubianes, M. D. *Electrochim. Acta* **2012**, *71*, 73−81.
(33) Gao, Q.; Sun, M.; Peng, P.; Qi, H.; Zhang, C. *Microchim. Acta* **2010**, *168*, 299−307.

(34) De Assis dos Santos Silva, F.; Lopes, C. B.; de Oliveira Costa, E.; Lima, P. R.; Kubota, L. T.; Goulart, M. O. F. *Electrochem. Commun.* **2010**, *12*, 450−454.
(35) Kumar, S.; Chen, S. *Sensors* **2008**, *8*, 739−766.
(36) Zhang, M.; Smith, A.; Gorski, W. *Anal. Chem.* **2004**, *76*, 5045−5050.
(37) Agüí, L.; Peña-Farfal, C.; Yáñez-Sedeño, P.; Pingarrón, J. M. *Electrochim. Acta* **2007**, *52*, 7946−7952.
(38) Deng, C.; Chen, J.; Chen, X.; Xiao, C.; Nie, Z.; Yao, S. *Electrochem. Commun.* **2008**, *10*, 907−909.
(39) Goran, J. M.; Favela, C. A.; Stevenson, K. J. *Anal. Chem.* **2013**, *85*, 9135−9141.
(40) Du, P.; Liu, S.; Wu, P.; Cai, C. *Electrochim. Acta* **2007**, *53*, 1811−1823.
(41) Moehlenbrock, M. J.; Meredith, M. T.; Minteer, S. D. *ACS Catal.* **2012**, *2*, 17−25.
(42) Hoshino, T.; Sekiguchi, S.; Muguruma, H. *Bioelectrochemistry* **2012**, *84*, 1−5.
(43) Kowalewska, B.; Kulesza, P. J. *Anal. Chem.* **2012**, *84*, 9564−9571.
(44) Villarrubia, C. W. N.; Garcia, S. O.; Lau, C.; Atanassov, P. *ECS J. Solid State Sci. Technol.* **2013**, *2*, M3156−M3159.
(45) Narváez Villarrubia, C. W.; Rincón, R. a; Radhakrishnan, V. K.; Davis, V.; Atanassov, P. *ACS Appl. Mater. Interfaces* **2011**, *3*, 2402−2409.
(46) Liu, S.; Cai, C. *J. Electroanal. Chem.* **2007**, *602*, 103−114.
(47) Tsai, Y.-C.; Chen, S.-Y.; Liaw, H.-W. *Sens. Actuators B* **2007**, *125*, 474−481.
(48) Meng, L.; Wu, P.; Chen, G.; Cai, C.; Sun, Y.; Yuan, Z. *Biosens. Bioelectron.* **2009**, *24*, 1751−1756.
(49) Mao, X.; Wu, Y.; Xu, L.; Cao, X.; Cui, X.; Zhu, L. *Analyst* **2011**, *136*, 293−298.
(50) Pelster, L. N.; Meredith, M. T.; Minteer, S. D. *Electroanalysis* **2012**, *24*, 1011−1018.
(51) Heller, A. *Acc. Chem. Res.* **1990**, *23*, 128−134.
(52) Heller, A. *J. Phys. Chem.* **1992**, *96*, 3579−3587.
(53) Lyon, J. L.; Stevenson, K. J. *Langmuir* **2007**, *23*, 11311−11318.
(54) Li, H.; Worley, K. E.; Calabrese Barton, S. *ACS Catal.* **2012**, *2*, 2572−2576.
(55) Bard, A. J.; Faulkner, L. R. *Electrochemical Methods: Fundamentals and Applications*, 2nd ed.; John Wiley and Sons: New York, 2001; pp 335−348.
(56) Aizawa, M.; Coughlin, R.; Charles, M. *Biochim. Biophys. Acta* **1975**, *385*, 362−370.
(57) Zare, H.; Golabi, S. *J. Solid State Electrochem.* **2000**, *4*, 87−94.
(58) Prasannakumar, S.; Manjunatha, R.; Nethravathi, C.; Suresh, G. S.; Rajamathi, M.; Venkatesha, T. V. *J. Solid State Electrochem.* **2012**, *16*, 3189−3199.
(59) Santhiago, M.; Lima, P. R.; Santos, W. D. J. R.; Oliveira, A. B. De; Kubota, L. T. *Electrochim. Acta* **2009**, *54*, 6609−6616.
(60) Saleh, F. S.; Rahman, M. R.; Kitamura, F.; Okajima, T.; Mao, L.; Ohsaka, T. *Electroanalysis* **2011**, *23*, 409−416.
(61) Saleh, F. S.; Okajima, T.; Kitamura, F.; Mao, L.; Ohsaka, T. *Electrochim. Acta* **2011**, *56*, 4916−4923.
(62) Zhao, L.; He, R.; Rim, K. T.; Schiros, T.; Kim, K. S.; Zhou, H.; Gutiérrez, C.; Chockalingam, S. P.; Arguello, C. J.; Pálová, L.; Nordlund, D.; Hybertsen, M. S.; Reichman, D. R.; Heinz, T. F.; Kim, P.; Pinczuk, A.; Flynn, G. W.; Pasupathy, A. N. *Science* **2011**, *333*, 999−1003.
(63) Maldonado, S.; Morin, S.; Stevenson, K. J. *Carbon* **2006**, *44*, 1429−1437.
(64) Maldonado, S.; Morin, S.; Stevenson, K. J. *Analyst* **2006**, *131*, 262−267.
(65) Wiggins-Camacho, J. D.; Stevenson, K. J. *J. Phys. Chem. C* **2009**, *113*, 19082−19090.
(66) Goran, J. M.; Stevenson, K. J. *Langmuir* **2013**, *29*, 13605−13613.
(67) Ciolkosz, M.; Jordan, J. *Anal. Chem.* **1993**, *65*, 164−168.